INTERNATIONAL JOURNAL OF HYDROGEN ENERGY 45 (2020) 9268–9277

Available online at www.sciencedirect.com

ScienceDirect

journal homepage: www.elsevier.com/locate/he

Enhanced adsorption sites in monolayer MoS_2 pyramid structures for highly sensitive and fast hydrogen sensor

Abhay V. Agrawal [a], *R. Kumar* [b], *Guang Yang* [c], *Jiming Bao* [c], *Mahesh Kumar* [b], *Mukesh Kumar* [a,*]

[a] *Functional and Renewable Energy Materials Laboratory, Indian Institute of Technology Ropar, Punjab, 140001, India*

[b] *Department of Electrical Engineering, Indian Institute of Technology Jodhpur, Jodhpur, 342011, India*

[c] *Department of Electrical and Computer Engineering, University of Houston, Houston, TX, 77204, USA*

HIGHLIGHTS

- Enhanced adsorption of H_2 gas on monolayer MoS_2 pyramids for H2 sensing.
- Least response time, high sensitivity and fast recovery of bare MoS_2 for H_2 sensing.
- High sensitivity of 24% for 0.1% H_2 by monolayer MoS_2 pyramid structures.
- Verification of favourable H_2 adsorption sites by the DFT results reported.

ARTICLE INFO

Article history:
Received 28 August 2019
Received in revised form
20 December 2019
Accepted 17 January 2020
Available online 9 February 2020

Keywords:
Mixed MoS_2 flakes
Pyramids like MoS_2 flakes
Edge-oriented MoS_2 flakes
Hydrogen sensor
CVD
In-plane MoS_2

ABSTRACT

Here, we present a highly sensitive and fast hydrogen (H_2) sensor for 1% H_2, well below the critical limit of explosion ignite in air, in a temperature range of 28–150 °C by using monolayer MoS_2 pyramid structures with enhanced adsorption sites. The monolayer MoS_2 pyramid structures is synthesized by modified chemical vapor deposition technique and characterized by field emission scanning electron microscopy, Raman, photoluminescence and atomic force microscopy. The highest sensitivity of 69.1% was achieved at a moderate temperature with a response time of 32.9 s for the monolayer MoS_2 pyramid structures. At room temperature (RT), the sensor showed a sensitivity of 6% with a faster response of 11.3 s and recovery time of 125.3 s. The availability of favourable adsorption sites on in-plane MoS_2 and edges of MoS_2 in monolayer MoS_2 structures provide enhanced adsorption sites for gas sensing and resulted in the high sensitivity and low response time compared to that of bare MoS_2 and other nanostructures-based H_2 sensor. The detailed gas sensing mechanism is proposed in the light of detail surface morphology and density function theory (DFT). This study reveals that tailoring the favourable adsorption sites in 2D materials is helpful to develop the highly sensitive and fast H_2 sensor for next generation safety devices for H_2 fueled vehicle and clean energy applications.

* *Corresponding author.*
E-mail address: mkumar@iitrpr.ac.in (M. Kumar).

https://doi.org/10.1016/j.ijhydene.2020.01.119

Introduction

Recently, hydrogen (H_2) based energy sources emerged as a potential candidate for production of clean and renewable energy, which is considered as the next generation energy source [1]. H_2 energy has been significantly attractive to the worldwide community due to its very high heat combustion (142 kJ/g). Moreover, it also provide independence from limited fossils fuels, and produce clean combustion product compared to those produced by nonrenewable energy sources [2,3]. Nowadays, H_2 gas is broadly used in many areas like chemical, aero-scope, space transportation, oil refining industries and medicine. However, H_2 is extremely explosive and flammable gas if its concentration is greater than 4% over environment volume due to its low ignition energy (0.017 mJ). Hence, a small leakage of the H_2 in any system is very dangerous and detrimental to the safe operation of H_2. Thus, in order to find leakages before a hazardous situation occurs, a highly sensitive, selective, fast recovery and responsive H_2 gas sensor is required.

Over the past few years, semiconducting molybdenum disulfide (MoS_2), a promising member of the transition metal dichalcogenides family has been intensively become the focus of the research community. MoS_2 has exceptional electronic, sensing, optical, catalytic and biological properties [4–6]. MoS_2 consists of the stacked three atoms thick layers bounded by strong covalent bonds and a weak interlayer van der Waals bonds [7]. Bulk MoS_2 has the indirect bandgap of 1.2 eV, which converts to a direct bandgap of 1.8 eV when bulk MoS_2 is thinned down to one layer [7,8]. Due to the higher direct band gap (1.8 eV), faster charge transport, higher surface to volume ratio and higher electron concentration at the surface, MoS_2 has gained tremendous interest for the development of next generation memory devices, solar cells and photodetectors [9–12].

Moreover, MoS_2 has inherent electrical, physical and chemical properties for gas sensing applications [13]. MoS_2 has higher surface-to-volume ratio and an easy way to control adsorption sites in comparison to traditional sensors [14,15]. Recently, the research community has continuously developed H_2, NO_2, NH_3, and H_2S gas sensors based on MoS_2 [16–18]. There are some important parameters like sensitivity, response and recovery time to elucidate the performance of the any gas sensor. The sensitivity is defined as ratio of change in resistance after gas exposure to resistance in presence of air $(\frac{R_{gas}-R_{air}}{R_{air}}) \times 100\%$ where R_{gas} and R_{air} is the resistance in presence of H_2 and air, respectively. The response time is defined as time required for a sensor to change resistance from 10 to 90% and recovery time is the time required to decay resistance from 90 to 10% of overall change.

However, bare MoS_2 based H_2 gas sensors suffered from long response time, long recovery time and low sensitivity, which is quite impractical for fast detection of H_2 gas [3,19–21]. Moreover, these parameters are enhanced by forming MoS_2 heterostructures with metal nanoparticles, Carbon nanotubes, TiO_2, reduced graphene (rGO) and graphene [22–28]. These strategies improved sensing performance, but also lead to increase complexity in device manufacturing [28–31].

In a chemiresistive gas sensor, gas molecules interact/adsorb on the sensing materials and charge transfer takes place between them. This charge transfer induces the change in the electrical resistance of the sensing materials. It has been reported that the gas adsorption is strongly dependent on the particular favourable sites on MoS_2 flakes [22,32,33]. The researchers focused to enhance the favourable adsorption sites of bare MoS_2 by modified growth and orientation of MoS_2 [16,18,34]. However, these in-plane MoS_2 or edge-enriched MoS_2 based sensor either suffered from low sensitivity or higher response and recovery time.

Here, we developed H_2 gas sensor based on monolayer MoS_2 pyramid structures. The height of monolayer MoS_2 pyramids varied from 3 to 25 nm stacked in-plane layers and the top of the pyramids have edge-oriented flakes with a height between 3 and 6 nm. We studied the sensing behavior of sensor down to 1% H_2 gas in the temperature range of 28–150 °C. We observed the highest sensitivity of 69.1% at moderate temperature with a response and recovery time of 32.9 and 141.8 s, respectively. At moderate temperature, sensor also showed a good sensitivity of 24% down to 0.1% of H_2. At RT, the sensor showed significant sensitivity of 6% with fast response and recovery time of 11.3 and 125.3 s, respectively. We proposed that our response time is shorter for a bare MoS_2 based H_2 sensor due to availability of enhanced favourable adsorption sites on in-plane flakes as well as on edges of monolayer MoS_2 pyramid structures. This study revealed that increase in favourable adsorption sites could lead to a fast response and highly sensitive RT H_2 gas sensor.

Experimental section

Synthesis of monolayer MoS_2 pyramids structures

Monolayer MoS_2 pyramids with edge-oriented top flakes fabricated on SiO_2/Si substrate by using modified chemical vapor deposition (CVD) techniques. The sulphur (99.8%, Sigma Aldrich) and MoO_3 (99.8%, Sigma Aldrich) powder were used for the growth of MoS_2 layers. We used the modified three zone chemical vapor deposition technique to grow the monolayer MoS_2 pyramid with edge-oriented top flakes and a small quartz tube closed at one end of the small quartz tube. The small tube was placed inside the big quartz tube in such a way that the close end of the small tube faced in-gas flow. The sulphur powder was placed at the open end in zone 2 and MoO_3 powder was placed in zone 1 at the closed end. The schematic of the experimental setup is shown in Fig. 1(a) and the temperature profile is shown in Fig. 1(b). The growth temperature for the sulphur and MoO_3 powder was 350 °C and 800 °C. The growth time of the deposition was 5 min followed by the natural cooling of CVD. We kept the argon gas flow 175 sccm than slowly decrease up to 100 sccm.

Characterization

The synthesized monolayer MoS_2 pyramids were characterized by field emission scanning electron microscope (FE-SEM), photoluminescence (PL), Raman and atomic force microscopy (AFM). The PL and Raman spectroscopy were performed by

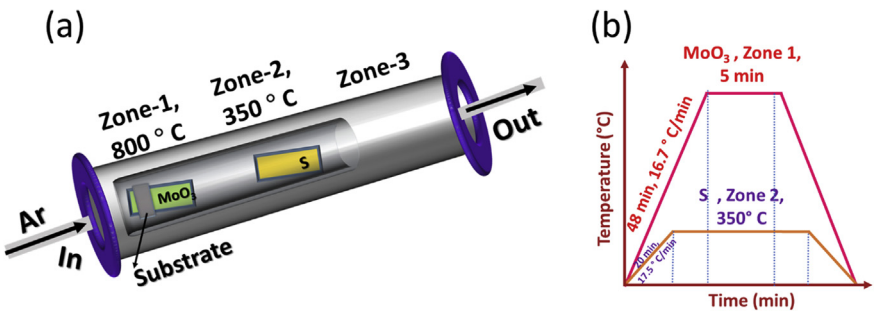

Fig. 1 – (a) Schematic of the modified chemical vapor deposition technique. (b) Temperature profile for the growth of monolayer MoS_2 pyramid structures.

HORIBA iHR 320 spectrometer with a home built optical microscope setup with 532 nm laser at fixed power of ~1 mW and a spot size of 1 μm. The circular Au/Cr metal contacts of 250/5 nm thick and having diameter 100 μm with separation of 500 μm each was deposited by thermal evaporation. The H_2 gas was diluted with Ar gas to test at different concentration in home-build setup. 1% H_2 gas concentration mixed with 99% argon was mixed in a home-built gas setup. The sensing measurements were done by computer controlled 4200 Keithley setup. The biasing voltage was fixed at 4 V during all the sensing measurements by a computer controlled Keithley 4200.

Results & discussion

Structure and morphological study

Fig. 2(a) shows the surface morphology of as-synthesized monolayer MoS_2 pyramid structures. The black region in FE-SEM image shows in-plane monolayer MoS_2 pyramids while white region on top of black pyramid shows edge-oriented MoS_2 flakes [16,18,34]. We further performed close view of completely developed MoS_2 pyramids shown in Fig. 2(b).

Fig. 2(c) shows an individual MoS_2 pyramid where growth of vertically aligned MoS_2 flakes just started. A small hump can be seen clearly in Fig. 2(c) which converts in complete vertically aligned MoS_2 structures with time. Some more FESEM images are added in supplementary information as Fig. S2 for better clarity. Two characteristic Raman peaks are observed at 387.4 and 412.3 cm^{-1} respectively corresponding to in-plane (E^1_{2g})and out of plane (A_{1g}) lattice vibrations of MoS_2 as shown in Fig. 2(d). [29, 30] The E^1_{2g} peak arises due to in-plane vibration of S and Mo atoms in opposite direction, while A_{1g} peak arises due to out of plane vibration of only S atoms, keeping Mo atom at rest. Thus, the peak intensity ratio A_{1g}/E^1_{2g} can be used to identify the orientation of MoS_2 flakes. The intensity ratio between A_{1g}/E^1_{2g} is 0.6 and ascertained that most of Raman intensity signals are corresponding to in-plane MoS_2 flakes [34–36]. Fig. 2(e) depicts the photoluminescence spectra of MoS_2 film and showed two prominent peaks at wavelength of 632.7 and 678.0 nm corresponding to B and A band exciton. These two peaks arise due to direct excitonic transfer between conduction band minimum to two split valence bands maximum. The valence band is split due to spin orbit coupling [37]. The crystal structure and phase identification has been done by the XRD. We observed the four sharp XRD peaks (002), (004), (101) and (006) at the 14.09°, 29.10°, 32.5°

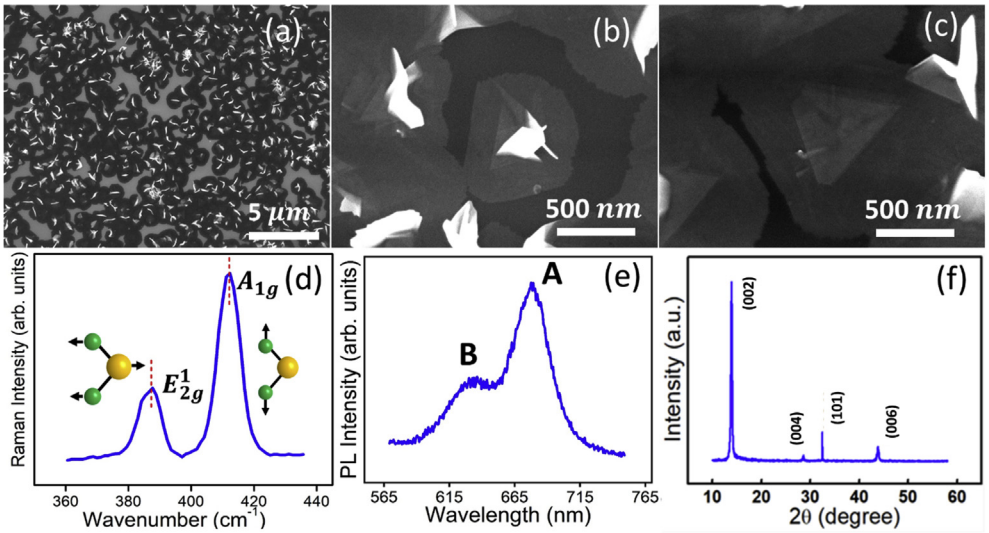

Fig. 2 – (a–c) FE-SEM image of monolayer MoS_2 pyramids with edge-oriented top flakes. (d) The Raman spectra of MoS_2 film with two well-known peaks corresponding to $E^1_{2g}$and A_{1g}vibrations. (e) PL spectra of MoS_2 film having B and A exciton peaks at 632.71 nm and 678.00 nm. (f) XRD spectra obtained from the film confirming the purity of the grown MoS_2 flakes.

and 44.05°. These peaks are well reported in vertical MoS_2 growth and can be indexed to hexagon phase of MoS_2 [38,39]. The XRD peaks for the MoS_2 further confirmed with JCPDS Card No. 37–1492. The synthesis of the MoS_2 flakes is a two-step process. (i) Reduction of MoO_3 in reduced MoO_2 (ii) Sulphurization of reduced MoO_2 to MoS_2 flakes. The possible chemical reactions are as follows:[34]

$$2MoO_3+S \rightarrow 2MoO_2+SO_2 \quad (1)$$

$$MoO_2+3S \rightarrow MoS_2+SO_2 \quad (2)$$

If there is any presence of reduced MoO_3, it should reflect in XRD. However, we did not observe any peak of reduced MoO_3. Thus, XRD spectra confirming the pure crystal structure of grown monolayer pyramid MoS_2 flakes.

The schematic of sensor device is shown in Fig. 3(a). When H_2 molecules were exposed to MoS_2 structures, they changed the resistance of the MoS_2 structures. We have studied the IV profile at RT and 150 °C with and without the H_2 exposure, shown in Fig. 3(b–c). We found that I–V curves are linear with and without H_2 exposure. The increase in current due to H_2 exposure is discussed in 3.3. The gas sensing measurements were performed with variable concentration of H_2 at different temperature range of 28 - 150 °C.

Hydrogen gas sensing study

Fig. 4(a) shows sensitivity vs time profile for all temperatures. The sensitivity is higher for higher temperature which implies increased interaction of H_2 gas molecules with monolayer MoS_2 pyramids at higher temperature. It is observed that the resistance decreases with increased H_2 exposure. Fig. 4(b) and (c) shows the response and recovery time of sensor. It can also be seen that lowest response time at RT is 11.3 s. The response time for other temperature ranges from 11.0 to 33.0 s. The calculation for response and recovery time is shown in Fig. 5(a–f) for the RT and at moderate temperature 150 °C. The current vs time graph for the RT and 150 °C is shown in Fig. 5 (a) and (d). It has been observed that the response time is increased with increase in the temperature from 28 to 150 °C. When H_2 gas molecules exposed to sensor, it adsorbed to favourable adsorption sites on the monolayer MoS_2 pyramids with edge oriented top flakes. At RT, the H_2 gas molecules easily adsorbed on the MoS_2 flakes and give response quickly. However, when the temperature of the device increases, the adsorption of H_2 gas is not so easy due to generated thermal energy. Atoms vibration in MoS_2 increases with increase in the temperature. At elevated temperature, now H_2 gas molecules need time to adsorb on the MoS_2 flakes in comparison to RT. Thus, the response time is also increased.

The nearly constant recovery time of 125–142 s implies that desorption of H_2 molecule is constant throughout all the temperatures. Fig. 4(d) depicts sensitivity profile of sensor. At RT, sensitivity of monolayer MoS_2 pyramids with edge-oriented top flakes is 6%. The sensitivity increased constantly and reached up to maximum sensitivity of 69.1% at 150 °C for 1% H_2. Higher temperature leads to increased diffusivity of H_2 molecule which increases sensitivity correspondingly In the present study, we studied the H_2 sensing performance from 28 to 150 °C. Kumar et al.; studied the H_2 sensing response from reverse biased MoS_2/GaN heterojunction in the temperature range from 25 to 180 °C [40]. The authors achieved the highest sensitivity at 150 °C. Beyond 150 °C, the H_2 sensing performance was decreased. The decreased sensitivity was attributed to dominate desorption rate of H_2 gas over the diffusion process. Moreover, in present study, the sensitivity increases from 28 °C to 125 °C rapidly from 6% to 66%. However, at higher temperature from 125 °C to 150 °C, the sensitivity is increase from 66% to 69%. At higher temperature beyond 100 °C, the device showed nearly constant increase in sensitivity. Hence, we study the device sensing behaviour from 28 to 150 °C. Also, our priority was to develop the H_2 sensor at lower temperature and ideally to work at RT. Hence, we study the device sensing behaviour from 28 to 150 °C. We have compared our results with other traditional metal oxides, bare MoS_2, MoS_2 hybrid and metal particle decorated sensor in Table 1. The combination of high sensitivity and low response time for our H_2 sensor at RT and moderate temperature is better than metal oxide nanostructures and any other bare MoS_2 H_2 sensor reported in literatures [41]. Our fabricated device also showed a very low response time in all temperature ranges even at RT compared to other bare MoS_2 based sensors [16,24,30,42,43].

The sensitivity for vertical MoS_2–Si heterostructure was reported to be ~685%; however, the reported sensor was nearly 10 time slower than our H_2 sensor [43]. The observed response time for monolayer MoS_2 pyramids is even better than our previous H_2 sensor on edge-enriched MoS_2 flakes with enhanced sensitivity at RT and at moderate temperature.

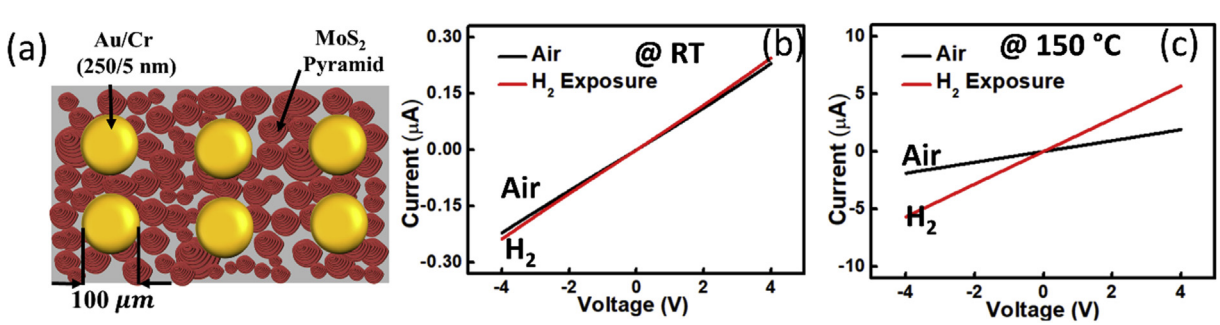

Fig. 3 – (a) Schematic of the gas sensing device. (b) IV curve with and without H_2 exposure at RT and (c) at 150 °C. IV curve clearly showed that the device behaves as the linear and the ohmic behavior with and without H_2 exposure.

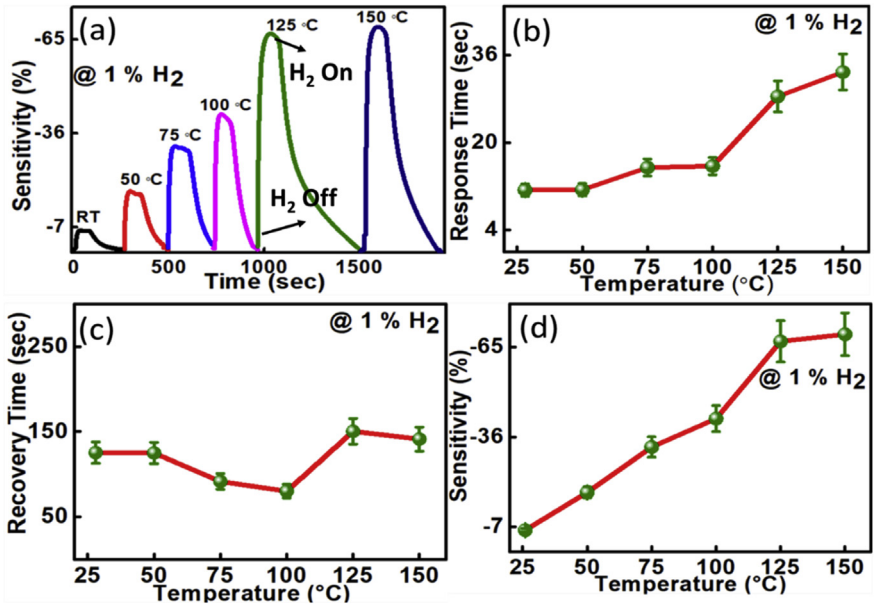

Fig. 4 – (a) Sensitivity vs time profile at different temperatures. (b) Response time profile (c) Recovery time profile (d) Sensitivity of monolayer MoS_2 pyramids with edge-oriented top flakes in the temperature range 28–150 °C.

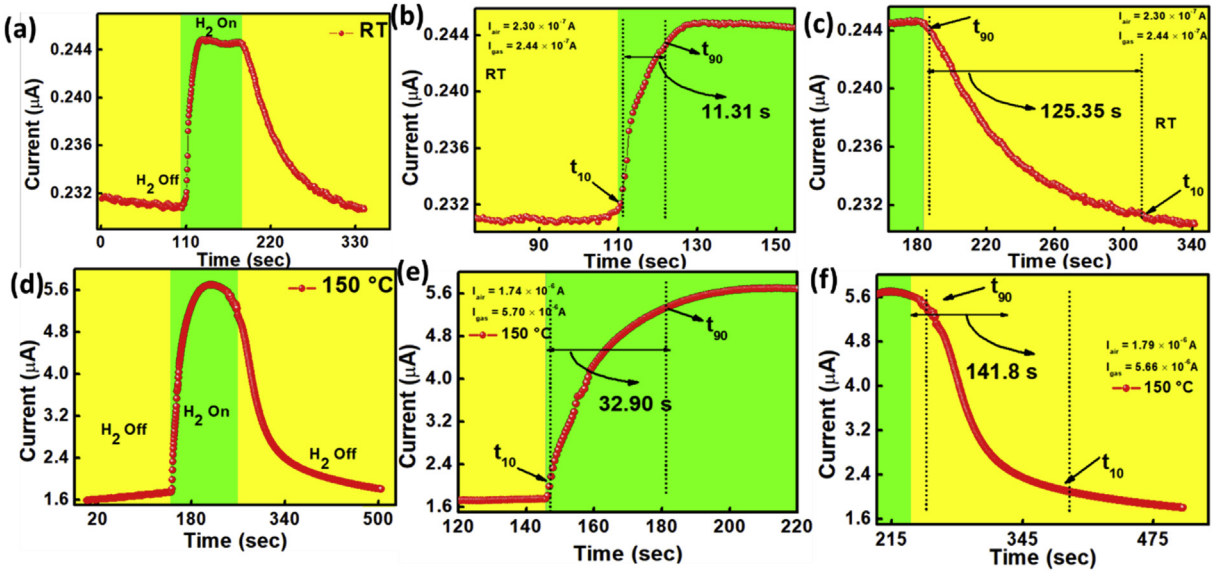

Fig. 5 – Calculation of response time and recovery time at (a–c) RT (d–f) at 150 °C for the 1% concentration of H_2 gas.

Hydrogen gas sensing mechanism

To understand the high sensitivity and low response time of our monolayer MoS_2 pyramidal structures, we investigated the detail surface morphology of monolayer MoS_2 pyramids. We did AFM measurements to study surface topography of grown structures. The AFM analysis is shown in Fig. 6(a).

Surface topography of MoS_2 film clearly shows layer by layer growth of monolayer MoS_2. To gain more insight into the growth, we studied the line profile of grown pyramid MoS_2 flakes and the result is shown in Fig. 6(b). A step like growth pattern is obtained from the line profile. Moreover, we also observed a sudden increase in the line profile at the top of these stacked layer. The number of stacked in-plane layers is 8–30 monolayer with the height of 5–20 nm. Fig. 6(c) shows zoomed area of the line profile. The height of single layer pyramid is around 0.7 nm which implies each stack is monolayer MoS_2 flakes. At the top, growth of edge-oriented MoS_2 takes place which confirmed from sudden increase in height of line profile. The height of edge-oriented flakes is varied from 3 to 7 nm. The surface morphology and step like line profile shown in Fig. 6(a–c) revealed pyramid like growth of MoS_2 structure. The line profile shows that size of individual island varied from 1 to 2 μm and the uncovered in-plane region on each monolayer pyramid varied from 20 to 30 nm, as shown in Fig. 6(c). Thus, this modified growth method

Table 1 – Summarized literature of different sensing materials based H_2 gas sensor.

S. No.	Materials	T (° C)	Res. Time (sec)	Rec. Time (sec)	S (%)	Ref.
1	Graphene/ZnO composite	100	96.0	190.0	2.0	[24]
2	Vertical MoS_2/Si heterojunction	RT	108.7	101.9	685.7	[43]
3	Graphene Palladium	RT	–	600	7	[44]
4	Graphene decorated Pd–Ag nanoparticles	RT	56	–	16.2	[45]
5	Nano-bitter CuO	200	150	1016	175	[46]
6	PdO loaded WO3	RT	126	348	8.02	[47]
7	Pd–Pt/WO_3 nanowires	RT	180	240	1.12	[48]
8	GaN	500	22.0	26.0	101.5	[49]
9	Porous MoS_2 microspheres	120	30.0	60.0	27.5	[23]
10	Edge - Enriched MoS_2	RT	14.3	136.8	1.0	[16]
11	Pt Functionalized PdO NWs	RT	166	–	62.0	[50]
12	rGO-MoS_2 nanoparticles	60	15.6	251	260	[51]
13	ZnO Nanowire	250	60	14	98%	[52]
14	SnO_2 nanowires	300	>100	60	–	[53]
15	TiO_2	180	131	68	18	[54]
16	In_2O_3	260	1.7	1.5	18	[55]
17	Pt/TiO_2/RGO	180	54	48	46	[54]
18	Pd–C core-shell nanoparticles	150	42	23	38	[56]
19	Pd/TiO_2/RGO	180	18	29	92	[54]
20	ZnO Single Nanorod	RT	30–40	50–90	4	[57]
21	Monolayer MoS_2 pyramid	RT	11.3	125.3	6	Present work
22	Monolayer MoS_2 pyramid	150	32.9	141.8	69.1	Present work

provides more favourable adsorption sites as well as a higher surface area in monolayer MoS_2 pyramid structures for H_2 molecule interaction. A 3D schematic of monolayer MoS_2 pyramids with edge-oriented top flakes is shown in Fig. 6(d).

The deposition rate, growth rate and sulphur rich environment are the important parameter to grow these special structures. Here, we first create sulphur rich environment in the small tube which plays vital role to synthesize MoS_2 flakes [58]. It is reported that closed end of the tube has very small gas velocity at closed end in comparison to open end of the tube [59]. Thus, MoS_2 vapor formed by the vaporization of the S and MoO_3 powder deposited slowly on the substrate.

Initially, we heat the sulphur powder first to create sulphur rich environment. For the growth of monolayer MoS_2 pyramids, Sulphur and MoO_3 react with each other and form MoS_2 vapors. Vaporized MoS_2 condensed on substrate and form in-plane monolayer MoS_2. With increase in growth time, more incoming MoS_2 vapors start condensing on the substrate and form isolated islands. Incoming atoms/molecules nucleate and formed first, second, third stacked on islands stacked.

Therefore, after a certain critical thickness of in-plane MoS_2 flakes, other factors like strain and screw dislocation may take place in the MoS_2 film. These factors restrict the growth direction in the in-plane. Thus, the growth direction of MoS_2 film changes from in-plane to vertical aligned direction [58]. The islands developed on whole substrate and formed monolayer MoS_2 pyramids with edge-oriented top flakes following the Stranski Krastanov growth model.[34,60] The growth of monolayer pyramids reveals the stacked monolayer and large number of exposed atomic edges [61]. Hence, with these monolayer pyramids not only the exposed area is increased but also large number of favourable adsorption sites are increased which enhanced H_2 gas adsorption. Therefore, in our case we controlled the surface reaction rate and mass transfer rate by controlling the gas flow [34]. Thus, tube in tube arrangement provide the slow and controlled sulphurization of the MoS_2 flakes on the substrate and plays an important role to achieve monolayer MoS_2 pyramid structures [58,62].

We proposed H_2 sensing mechanism based on the preferential and enhanced adsorption sites for H_2 of monolayer MoS_2 pyramids. The gas molecules adsorption on MoS_2 is highly position dependent [33]. The gas molecule interaction is examined by adsorption energy and charge transfer between MoS_2 and gas molecules at different sites. It has been well reported theoretically and experimentally that gas molecules adsorption on MoS_2 can be happen on four adsorption sites top of hexagon (H), top of Mo atoms (T_M), top of S atoms (T_S), and top of Mo–S bonds (B) as shown in Fig. 6(d) [63,64]. The adsorption energy calculated by $E_a = E_{MoS_2+molecule} - (E_{MoS_2} + E_{molecule})$. Here, $E_{MoS_2+molecule}$ is total adsorption energy of jointly formed MoS_2 and H_2 gas molecule bonded on it. E_{MoS_2} and $E_{molecule}$ are total energy of individual MoS_2 and H_2 gas molecule, respectively [63]. For favourable adsorption of gas molecule, the adsorption energy should be negative and the reaction is exothermic in nature. The highest negative adsorption energy of a sensing material for a particular gas implies more selective and sensitive nature of the material for that gas. Another important parameter is the electron transfer between gas molecules and MoS_2 flakes. If the electron transfers from gas molecule to MoS_2 then gas called as electron donor while if electron transfer from MoS_2 to gas molecule then gas called as electron acceptor. [63], Yue and his coworkers reported that possible adsorption sites on MoS_2 for H_2 gas molecules adsorption are T_M, H and T_S sites with theoretically calculated adsorption energies of −82 meV, −70 meV and −49 meV, respectively [63]. The H sites are highly probable at in-plane MoS_2 flakes while T_M and T_S sites are probable at edge-enriched MoS_2 flakes and on in-plane MoS_2 flakes. In another report by Ganji et al.; H_2 gas adsorption studied on MoS_2 and WS_2 flakes [64]. The adsorption energy for H_2

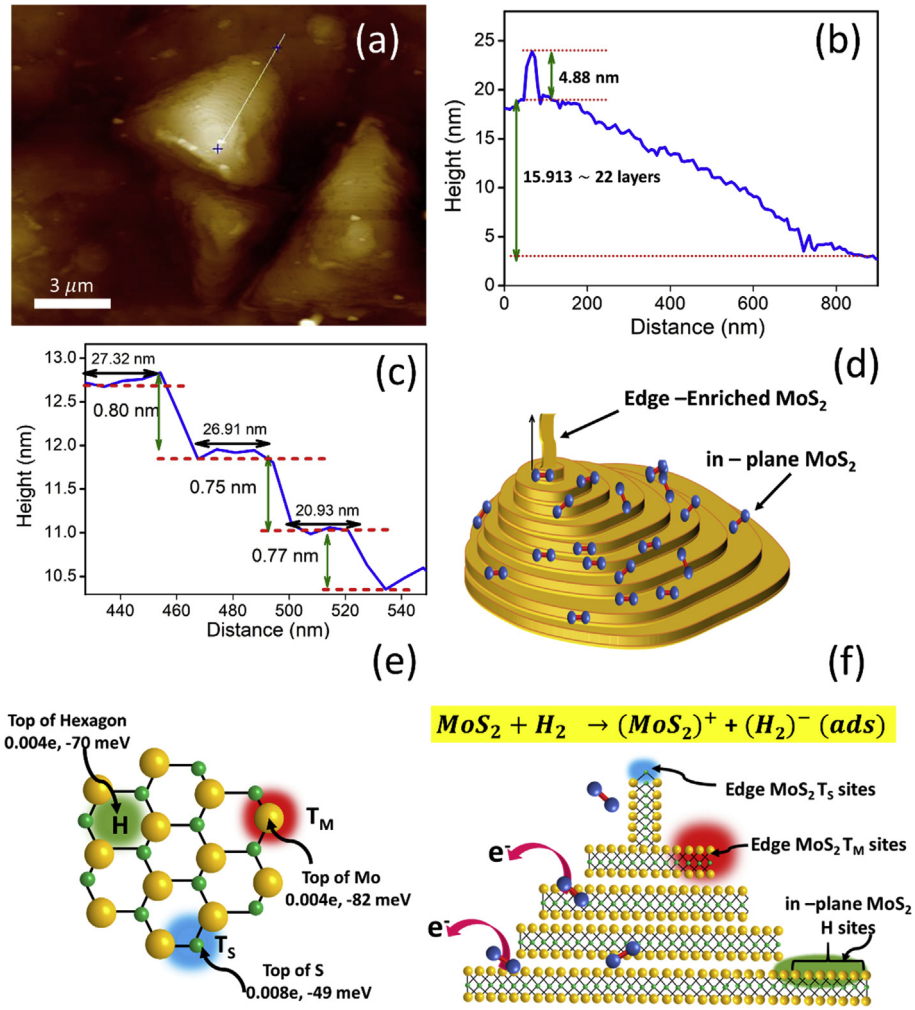

Fig. 6 – (a) AFM surface topography of monolayer MoS_2 pyramids with top edge-enriched flakes. (b) The line profile of as grown MoS_2 pyramids with edge-oriented top flakes. (c) The zoomed line profile which clearly shows thickness of each stacked layers is 0.7 nm correspond to monolayer and uncovered region of monolayers is varied from 20 to 30 nm (d) Schematic of the grown MoS_2 flakes. (e) Possible adsorption sites available on MoS_2 pyramids with edge-oriented top flakes and calculated adsorption energies and charge transfer at respective sites. (f) H_2 gas molecule interaction with MoS_2 pyramids with edge-oriented top flakes. H_2 interact with MoS_2 and takes the electron from MoS_2.

adsorption on MoS_2 is −131.61 meV at the top of Mo atoms. Moreover, authors found positive 0.004e charge transfer from MoS_2 to H_2 molecules. In our monolayer MoS_2 pyramid structures, we not only enhanced H site on stacked in-plane MoS_2 pyramids but also enhanced T_M and T_S sites on exposed edges simultaneously.

Also, it is clear that combination of these three sites on in-plane MoS_2 and edge-enriched MoS_2 in such a large extent is not possible. The stacked in-plane monolayer MoS_2 pyramids increases H sites and exposed edges of in-plane and edge-oriented flakes at top increases T_M and T_S sites [63]. The H_2 gas molecule interaction with MoS_2 pyramids having edge-oriented top flakes is shown in Fig. 6(e). Fig. 6(e) revealed that each stacked in-plane layer not only provides large surface area for H_2 gas interaction but also favourable in-plane and edge sites. The combination of T_M, H and T_S sites available in monolayer MoS_2 pyramids is mainly responsible for high sensitivity, fast response and comparatively low recovery time. Moreover, the net positive electron transfer from MoS_2 to H_2 molecules is 0.004e for both H sites and T_M sites and 0.008e at the T_S site; this also verified that H_2 has an electron acceptor nature for the MoS_2 [63]. The chemical reactions between the MoS_2 and H_2 gas molecules is shown in Fig. 6 (f). Exposed H_2 molecules are interacting with all layers from base to top in monolayer MoS_2 pyramids. The monolayer MoS_2 flakes provided all possible three combinations (H sites, T_S sites and T_M sites) of the favourable adsorption sites require for H_2 gas molecule adsorption. Thus, exposed H_2 gas molecules strongly adsorbed on the MoS_2 flakes. Hence, when H_2 gas turned off, H_2 gas molecules need time to desorbed from the monolayer MoS_2 pyramids. Which leads to high recovery time.

The electron acceptor nature of H_2 gas on MoS_2 flakes is also observed in our previous reports. We fabricated the highly dense vertical aligned MoS_2 flakes [16]. The vertical aligned MoS_2 flakes have the T_M and T_S sites only which is favourable adsorption sites for H_2 adsorption. The vertical aligned MoS_2 flakes showed n-type behaviour and when H_2

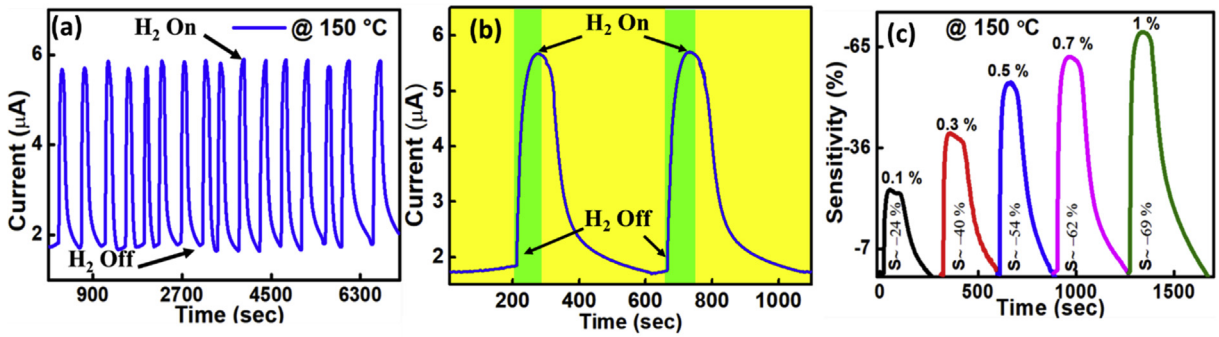

Fig. 7 – (a) Cyclability performance of monolayer MoS_2 pyramid structures sensor. (b) Zoomed View of first two cycles of cyclability data. (c) Dynamic plot for different concentrations of H_2 gas at 150 °C.

exposed to vertical aligned MoS_2 flakes, the resistance of the film is increased which also implies that H_2 gas takes electrons from vertical aligned MoS_2 flakes. The possible H_2 adsorption reactions between MoS_2 and H_2 gas molecules are as follows;

$$MoS_2 + H_2 \rightarrow (MoS_2)^+ + (H_2)^- \quad (3)$$

In another report, we studied the NO_2 sensing by utilizing the p type mixed MoS_2 flakes [18]. Mixed MoS_2 flakes have the combination of in-plane MoS_2 flakes and vertical aligned MoS_2 flakes. The favourable NO_2 adsorption sites in the mixed MoS_2 flakes are H sites, T_S site and B site. In this case of mixed MoS_2 flakes, we also studied the H_2 sensing performance on the mixed MoS_2 flakes. We again observed similar behaviour with H_2 gas. H_2 and NO_2 both behaves as the electron acceptor and the resistance of the film decreased. However, this time H_2 sensing performance has been decreased due to less availability of favourable adsorption sites in mixed MoS_2 flakes.

It is clear now that H_2 takes electron from MoS_2 film. However, resistance is decreased with H_2 exposure which implies that grown MoS_2 is of p-type in nature. This p -type behaviour can also be seen from IV curve taken at RT and 150 C shown in Fig. 3(b–c). The monolayer MoS_2 flakes with edge oriented top flakes having the p type nature, which implies MoS_2 flakes have the holes as the majority charge carrier while electrons as the minority charge carriers. When H_2 gas exposed to device, H_2 gas molecules withdraw the electron from p type MoS_2 flakes due to its electron acceptor nature. Hence majority of holes carriers increases in p type MoS_2 flakes which decreases the resistance of the films. Thus, the current is increased with H_2 exposure, as can be seen from Fig. 3(b–c).

The p type behaviour of monolayer MoS_2 pyramid structures may be attributed to the various defects and oxygen adsorption on the surface of MoS_2. In a report by Neal et al. the author predicted that a controlled adsorption of oxygen or interaction with MoS_2 may induce a p type doping. Furthermore, some other factors like defects generated during the synthesis of pyramid MoS_2 by chemical vapor deposition, charge interaction/transfer from the substrate, effect of metal semiconductor contact, annealing results in the controlled p type behaviour of MoS_2 flakes [18,65,66].

Finally, we did the cyclability and dynamic concentrations measurement to check the stability of the H_2 gas sensor. Cyclability is an important parameter to understand the stability of the chemiresistive gas sensor. The current vs time profile for the 16 cycles at 150 °C is shown in Fig. 7(a–b). We have tested the stability over the span of two months at all temperatures. We have observed that sensitivity is nearly constant for this sensor. The dynamic plot for the different concentrations is shown in Fig. 7(c). The H_2 concentration is varied from the 0.1, 0.3, 0.5, 0.7 and 1%. For the 0.1% H_2 concentration the sensitivity is 24%, which is quite high for such a low concentration of H_2 and shows the high sensitivity of sensor for even very low concentration of H_2.

Conclusion

In conclusion, we synthesized monolayer MoS_2 pyramid structures by modified CVD. Each pyramid consists 3–25 layers of in-plane monolayer MoS_2 flakes while capstone of each pyramid has edge-oriented MoS_2 flakes with a height from 3 to 7 nm. The uncovered region in each stacked layer is around 24–28 nm with size of each pyramid in the range of ~1–2 μm. The sensitivity of these pyramid MoS_2 flakes is 6% for 1% H_2 with a fast response time of 11.3 s at RT. Furthermore, the gas sensing mechanism based on DFT also confirmed that our proposed modified growth method is responsible for highly sensitive and fast detection of H_2 gas molecules on monolayer MoS_2 pyramids with edge-oriented top flakes. Monolayer MoS_2 pyramids with edge-oriented flakes at top provided highly favourable adsorption sites at top of hexagon (H), top of Mo atoms (T_M) and top of S atoms (T_S). We believe that proposed research work clearly provides more insight to understanding role of favourable adsorption sites to design a highly sensitive and fast H_2 sensor for safe operation of next generation H_2 based fuel systems.

Acknowledgement

The authors acknowledge financial support from the Department of atomic energy (DAE) under Project No. 34/September 20, 2015/BRNS and also the Department of Physics, IIT Ropar,

for providing experimental facility. J.M.B. acknowledges support from Welch Foundation (E-1728).

Appendix A. Supplementary data

Supplementary data to this article can be found online at https://doi.org/10.1016/j.ijhydene.2020.01.119.

REFERENCES

[1] Hydrogen on the rise. Nature Energy 2016;1:16127.
[2] Hübert T, Boon-Brett L, Black G, Banach U. Hydrogen sensors – a review. Sensor Actuator B Chem 2011;157(2):329–52.
[3] Crabtree GW, Dresselhaus MS, Buchanan MV. The hydrogen economy. Phys Today 2004;57(12):39–44.
[4] Siao MD, Shen WC, Chen RS, Chang ZW, Shih MC, Chiu YP, Cheng CM. Two-dimensional electronic transport and surface electron accumulation in MoS_2. Nat Commun 2018;9(1):1442.
[5] Mennel L, Furchi MM, Wachter S, Paur M, Polyushkin DK, Mueller T. Optical imaging of strain in two-dimensional crystals. Nat Commun 2018;9(1):516.
[6] Lee J, Dak P, Lee Y, Park H, Choi W, Alam MA, Kim S. Two-dimensional layered MoS_2 biosensors enable highly sensitive detection of biomolecules. Sci Rep 2014;4:7352.
[7] Mak KF, Lee C, Hone J, Shan J, Heinz TF. Atomically thin MoS_2: a new direct-gap semiconductor. Phys Rev Lett 2010;105.
[8] Masubuchi S, Morimoto M, Morikawa S, Onodera M, Asakawa Y, Watanabe K, Taniguchi T, Machida T. Autonomous robotic searching and assembly of two-dimensional crystals to build van der Waals superlattices. Nat Commun 2018;9(1):1413.
[9] Christian W, Shashank SH, Egbert Z. Controlling the electronic properties of van der Waals heterostructures by applying electrostatic design. 2D Mater 2018;5(3):035019.
[10] Lin S, Li X, Wang P, Xu Z, Zhang S, Zhong H, Wu Z, Xu W, Chen H. Interface designed MoS_2/GaAs heterostructure solar cell with sandwich stacked hexagonal boron nitride. Sci Rep 2015;5:15103.
[11] Gan LY, Zhang Q, Cheng Y, Schwingenschlögl U. Photovoltaic heterojunctions of fullerenes with MoS_2 and WS_2 monolayers. J Phys Chem Lett 2014;5:1445.
[12] Heiranian M, Farimani AB, Aluru NR. Water desalination with a single-layer MoS_2 nanopore. Nat Commun 2015;6:8616.
[13] Yang S, Jiang C, Wei S-h. Gas sensing in 2D materials. Appl Phys Rev 2017;4(2):021304.
[14] Kumar M, Mehta BR, Singh VN, Chatterjee R, Milikisiyants S, Lakshmi KV, Singh JP. The role of stoichiometry of indium and oxygen on gas sensing properties of indium oxide nanostructures. Appl Phys Lett 2010;96(12):123114.
[15] Liu Y, Hao L, Gao W, Xue Q, Guo W, Wu Z, Lin Y, Zeng H, Zhu J, Zhang W. Electrical characterization and ammonia sensing properties of MoS_2/Si p–n junction. J Alloys Compd 2015;631:105–10.
[16] Agrawal AV, Kumar R, Venkatesan S, Zakhidov A, Zhu Z, Bao J, Kumar M, Kumar M. Fast detection and low power hydrogen sensor using edge-oriented vertically aligned 3-D network of MoS_2 flakes at room temperature. Appl Phys Lett 2017;111(9):093102.
[17] Cho B, Hahm MG, Choi M, Yoon J, Kim AR, Lee YJ, Park SG, Kwon JD, Kim CS, Song M, Jeong Y, Nam KS, Lee S, Yoo TJ, Kang CG, Lee BH, Ko HC, Ajayan PM, Kim DH. Charge-transfer-based gas sensing using atomic-layer MoS_2. Sci Rep 2015;5:8052.
[18] Agrawal AV, Kumar R, Venkatesan S, Zakhidov A, Yang G, Bao J, Kumar M, Kumar M. Photoactivated mixed in-plane and edge-enriched p-type MoS_2 flake-based NO_2 sensor working at room temperature. ACS Sens 2018;3(5):998–1004.
[19] Maniyara RA, Mkhitaryan VK, Chen TL, Ghosh DS, Pruneri V. An antireflection transparent conductor with ultralow optical loss (<2 %) and electrical resistance (<6 Omega sq(-1)). Nat Commun 2016;7:13771.
[20] Stoddart A. Electronic devices: making multi-terminal memtransistors. Nature Reviews Materials 2018;3:18014.
[21] Gao J, Li B, Tan J, Chow P, Lu TM, Koratkar N. Aging of transition metal dichalcogenide monolayers. ACS Nano 2016;10(2):2628–35.
[22] Kathiravan D, Huang B-R, Saravanan A, Prasannan A, Hong P-D. Highly enhanced hydrogen sensing properties of sericin-induced exfoliated MoS_2 nanosheets at room temperature. Sensor Actuator B Chem 2019;279:138–47.
[23] Zhang Y, Zeng W, Li Y. The hydrothermal synthesis of 3D hierarchical porous MoS_2 microspheres assembled by nanosheets with excellent gas sensing properties. J Alloys Compd 2018;749:355–62.
[24] Anand K, Singh O, Singh MP, Kaur J, Singh RC. Hydrogen sensor based on graphene/ZnO nanocomposite. Sensor Actuator B Chem 2014;195:409–15.
[25] Zhao Y, Li W. Effect of annealing and HNO_3-treatment on the electrical properties of transparent conducting carbon nanotube films. Microelectron Eng 2010;87(4):576–9.
[26] Song J, Lou H. Improvement of gas-adsorption performances of Ag-functionalized monolayer MoS_2 surfaces: a first-principles study. J Appl Phys 2018;123(17):175303.
[27] Han SW, Cha G-B, Kang M, Lee JD, Hong SC. Hydrogen interaction with selectively desulfurized MoS_2 surface using Ne+ sputtering. J Appl Phys 2019;125(8):085102.
[28] Gong Y, Adhikari P, Liu Q, Wang T, Gong M, Chan W-L, Ching W-Y, Wu J. Designing the interface of carbon nanotube/biomaterials for high-performance ultra-broadband photodetection. ACS Appl Mater Interfaces 2017;9(12):11016–24.
[29] Hao L, Liu H, Xu H, Dong S, Du Y, Wu Y, Zeng H, Zhu J, Liu Y. Flexible Pd-WS_2/Si heterojunction sensors for highly sensitive detection of hydrogen at room temperature. Sensor Actuator B Chem 2019;283:740–8.
[30] Liu Y, Hao L, Gao W, Wu Z, Lin Y, Li G, Guo W, Yu L, Zeng H, Zhu J. Hydrogen gas sensing properties of MoS_2/Si heterojunction. Sensor Actuator B Chem 2015;211:537–43.
[31] Wang Q, Zhang W, Peng B, Zeng H, Zhang W. Spin to charge conversion at the conducting TiO2 surface. Phys Status Solidi Rapid Res Lett 2017;11(9):1700149.
[32] Cho S-Y, Kim SJ, Lee Y, Kim J-S, Jung W-B, Yoo H-W, Kim J, Jung H-T. Highly enhanced gas adsorption properties in vertically aligned MoS_2 layers. ACS Nano 2015;9(9):9314–21.
[33] Leenaerts O, Partoens B, Peeters FM. Adsorption of H_2O, NH_3, CO, NO_2, and NO on graphene: a first-principles study. Phys Rev B 2008;77.
[34] Agrawal AV, Kumar N, Venkatesan S, Zakhidov A, Manspeaker C, Zhu Z, Robles Hernandez FC, Bao J, Kumar M. Controlled growth of MoS_2 flakes from in-plane to edge-enriched 3D network and their surface-energy studies. ACS Applied Nano Materials 2018;1(5):2356–67.
[35] Lee C, Yan H, Brus LE, Heinz TF, Hone J, Ryu S. Anomalous lattice vibrations of single- and few-layer MoS_2. ACS Nano 2010;4:2695.
[36] Verble JL, Wieting TJ. Lattice mode degeneracy in Mo${\mathrm{S}}_{2}$ and other layer compounds. Phys Rev Lett 1970;25(6):362–5.

[37] Splendiani A, Sun L, Zhang Y, Li T, Kim J, Chim CY, Galli G, Wang F. Emerging photoluminescence in monolayer MoS_2. Nano Lett 2010;10(4):1271–5.
[38] Zhang S, Liu J, Ruiz K, Tu R, Yang M, Li Q, Shi J, Li H, Zhang L, Goto T. Morphological evolution of vertically standing molybdenum disulfide nanosheets by chemical vapor deposition. Materials 2018;11(4):631.
[39] Shokhen V, Miroshnikov Y, Gershinsky G, Gotlib N, Stern C, Naveh D, Zitoun D. On the impact of vertical alignment of MoS_2 for efficient lithium storage. Sci Rep 2017;7(1):3280.
[40] Goel N, Kumar R, Jain SK, Rajamani S, Roul B, Gupta G, Kumar M, Krupanidhi S. A high-performance hydrogen sensor based on a reverse-biased MoS_2/GaN heterojunction. Nanotechnology 2019;30(31):314001.
[41] Kumar M, Bhati VS, Kumar M. Effect of Schottky barrier height on hydrogen gas sensitivity of metal/TiO_2 nanoplates. Int J Hydrogen Energy 2017;42(34):22082–9.
[42] Baek D-H, Kim J. MoS_2 gas sensor functionalized by Pd for the detection of hydrogen. Sensor Actuator B Chem 2017;250:686–91.
[43] Hao L, Liu Y, Gao W, Liu Y, Han Z, Yu L, Xue Q, Zhu J. High hydrogen sensitivity of vertically standing layered MoS_2/Si heterojunctions. J Alloys Compd 2016;682:29–34.
[44] Phan D-T, Chung G-S. Characteristics of resistivity-type hydrogen sensing based on palladium-graphene nanocomposites. Int J Hydrogen Energy 2014;39(1):620–9.
[45] Sharma B, Kim J-S. Graphene decorated Pd-Ag nanoparticles for H_2 sensing. Int J Hydrogen Energy 2018;43(24):11397–402.
[46] Nakate UT, Lee GH, Ahmad R, Patil P, Hahn Y-B, Yu Y, Suh E-k. Nano-bitter gourd like structured CuO for enhanced hydrogen gas sensor application. Int J Hydrogen Energy 2018;43(50):22705–14.
[47] Geng X, Luo Y, Zheng B, Zhang C. Photon assisted room-temperature hydrogen sensors using PdO loaded WO_3 nanohybrids. Int J Hydrogen Energy 2017;42(9):6425–34.
[48] Choi J, Kim J. Highly sensitive hydrogen sensor based on suspended, functionalized single tungsten nanowire bridge. Sensor Actuator B Chem 2009;136(1):92–8.
[49] Hermawan A, Asakura Y, Kobayashi M, Kakihana M, Yin S. High temperature hydrogen gas sensing property of GaN prepared from α-GaOOH. Sensor Actuator B Chem 2018;276:388–96.
[50] Cho H-J, Chen VT, Qiao S, Koo W-T, Penner RM, Kim I-D. Pt-functionalized PdO nanowires for room temperature hydrogen gas sensors. ACS Sens 2018;3(10):2152–8.
[51] Venkatesan A, Rathi S, Lee I-y, Park J, Lim D, Kang M, Joh H-I, Kim G-H, Kannan E. Molybdenum disulfide nanoparticles decorated reduced graphene oxide: highly sensitive and selective hydrogen sensor. Nanotechnology 2017;28(36):365501.
[52] Sinha M, Mahapatra R, Mondal B, Maruyama T, Ghosh R. Ultrafast and reversible gas-sensing properties of ZnO nanowire arrays grown by hydrothermal technique. J Phys Chem C 2016;120(5):3019–25.
[53] Wang B, Zhu LF, Yang YH, Xu NS, Yang GW. Fabrication of a SnO_2 nanowire gas sensor and sensor performance for hydrogen. J Phys Chem C 2008;112(17):6643–7.
[54] Esfandiar A, Ghasemi S, Irajizad A, Akhavan O, Gholami M. The decoration of TiO_2/reduced graphene oxide by Pd and Pt nanoparticles for hydrogen gas sensing. Int J Hydrogen Energy 2012;37(20):15423–32.
[55] Li Z, Yan S, Wu Z, Li H, Wang J, Shen W, Wang Z, Fu Y. Hydrogen gas sensor based on mesoporous In2O3 with fast response/recovery and ppb level detection limit. Int J Hydrogen Energy 2018;43(50):22746–55.
[56] Singh V, Dhall S, Kaushal A, Mehta BR. Room temperature response and enhanced hydrogen sensing in size selected Pd-C core-shell nanoparticles: role of carbon shell and Pd-C interface. Int J Hydrogen Energy 2018;43(2):1025–33.
[57] Lupan O, Chai G, Chow L. Novel hydrogen gas sensor based on single ZnO nanorod. Microelectron Eng 2008;85(11):2220–5.
[58] Kumar P, Viswanath B. Effect of sulfur evaporation rate on screw dislocation driven growth of MoS_2 with high atomic step density. Cryst Growth Des 2016;16(12):7145–54.
[59] Wang C, Chen W, Han C, Wang G, Tang B, Tang C, Wang Y, Zou W, Chen W, Zhang X-A, Qin S, Chang S, Wang L. Growth of millimeter-size single crystal graphene on Cu foils by circumfluence chemical vapor deposition. Sci Rep 2014;4:4537.
[60] Thin films — a historical perspective A2 - ohring, milton. In: The materials science of thin films. San Diego: Academic Press; 1992 [pp xix-xx].
[61] Michely T, Krug J. Islands, mounds and atoms, vol. 42. Springer Science & Business Media; 2012.
[62] Lin X, Liu Y, Wang K, Wei C, Zhang W, Yan Y, Li YJ, Yao J, Zhao YS. Two-dimensional pyramid-like WS_2 layered structures for highly efficient edge second-harmonic generation. ACS Nano 2018;12(1):689–96.
[63] Yue Q, Shao Z, Chang S, Li J. Adsorption of gas molecules on monolayer MoS_2 and effect of applied electric field. Nanoscale Research Letters 2013;8(1):425.
[64] Ganji MD, Sharifi N, Ghorbanzadeh Ahangari M, Khosravi A. Density functional theory calculations of hydrogen molecule adsorption on monolayer molybdenum and tungsten disulfide. Phys E Low-dimens Syst Nanostruct 2014;57:28–34.
[65] Dolui K, Rungger I, Sanvito S. Origin of the n-type and p -type conductivity of MoS_2 monolayers on a SiO_2 substrate. Phys Rev B 2013;87(16):165402.
[66] Neal AT, Pachter R, Mou S. P-type conduction in two-dimensional MoS_2 via oxygen incorporation. Appl Phys Lett 2017;110(19):193103.